7. Data Report: Composition of Clay Minerals from Hemipelagic Sediments at Hydrate Ridge, Cascadia Subduction Zone[1]

Michael Underwood[2] and Marta Torres[3]

ABSTRACT

This report describes the results of semiquantitative analysis of clay mineral composition by X-ray diffraction. The samples consist of hemipelagic mud and mudstone cored from Hydrate Ridge during Leg 204 of the Ocean Drilling Program. We analyzed oriented aggregates of the clay-sized fractions (<2 μm) to estimate relative percentages of smectite, illite, and chlorite (+ kaolinite). For the most part, stratigraphic variations in clay mineral composition are modest and there are no significant differences among the seven sites that were included in the study. On average, early Pleistocene to Holocene trench slope and slope basin deposits contain 29% smectite, 31% illite, and 40% chlorite (+ kaolinite). Late Pliocene to early Pleistocene strata from the underlying accretionary prism contain moderately larger proportions of smectite with average values of 38% smectite, 27% illite, and 35% chlorite (+ kaolinite). There is no evidence of clay mineral diagenesis at the depths sampled. The expandability of smectite is, on average, equal to 64%, and there are no systematic variations in expandability as a function of burial depth or depositional age. The absence of clay mineral diagenesis is consistent with the relatively shallow sample depths and corresponding maximum temperatures of only 24°–33°C.

[2] Department of Geological Sciences, University of Missouri, Columbia MO 65211, USA.
UnderwoodM@missouri.edu
[3] College of Oceanic and Atmospheric Sciences, Oregon State University, Corvalis OR 97331, USA.

INTRODUCTION

Hydrate Ridge is one of the more prominent bathymetric features along the central Cascadia accretionary complex, measuring 25 km long × 15 km wide (Fig. F1). Offscraped sedimentary strata beneath the ridge have been transferred from the subducting Juan de Fuca plate and include large volumes of sandy and silty turbidites (Kulm and Fowler, 1974; MacKay et al., 1992; Underwood et al., 2005). Previous sampling expeditions demonstrated that the overlying slope and slope basin deposits of Cascadia tend to be finer grained and thinner bedded than the underlying accreted strata (Kulm and Fowler, 1974; Barnard, 1978; Kulm and Scheidegger, 1979; Shipboard Scientific Party, 1994a, 1994b). The Ocean Drilling Program (ODP) returned to the Hydrate Ridge area during Leg 204 to determine how biogeochemical factors control the distribution and concentration of gas hydrates (Shipboard Scientific Party, 2003). In this data report, we document how the common clay minerals in hemipelagic mud and mudstone (smectite, illite, and chlorite) change in relative abundance near Hydrate Ridge. The original goal of our investigation was to determine whether any of the variations in shipboard pore water geochemistry (Shipboard Scientific Party, 2003) could be attributed to systematic or sporadic shifts in the detrital composition or alteration of the mineral matrix. Of secondary interest was whether clay mineral composition changes as a function of depositional age or lithostratigraphy.

Nine sites were cored during ODP Leg 204 (Fig. F1), but we analyzed samples from only seven of those sites (Fig. F2). Stratigraphic correlations between and among the sites follow several prominent seismic reflectors (e.g., Reflector Y and Reflector A) and datable biostratigraphic events (e.g., diatoms and nannofossils). Shipboard scientists subdivided the trench slope and slope basin deposits into lithostratigraphic units on the basis of variations in texture, mineral and microfossil composition, and physical properties (Shipboard Scientific Party, 2003). In general, the slope deposits thin and fine upward. Because of progressive subduction-induced deformation, however, acoustic expression of the structural boundary between trench slope deposits and the underlying accretionary prism is not everywhere distinct (Fig. F3). Increases in the degree of induration and in the proportion of turbidite sand-silt indicate that boreholes penetrated the tectonostratigraphic boundary at Sites 1244, 1245, and 1251 (Fig. F2).

X-RAY DIFFRACTION METHODS

Analyses of sediment samples by X-ray diffraction (XRD) have been a routine part of shipboard and shore-based measurements by the ODP and the Deep Sea Drilling Project (DSDP). The presence of a specific detrital and/or authigenic mineral can be detected easily through visual recognition of characteristic peak positions. It is more problematic, however, to estimate the relative abundance of a mineral in bulk sediment with meaningful accuracy (Moore, 1968; Cook et al., 1975; Heath and Pisias, 1979; Johnson et al., 1985; Fisher and Underwood, 1995; Underwood et al., 2003). The most common approach for analyzing marine clays has been to apply the Biscaye (1965) peak area weighting factors (smectite = 1×, illite = 4×, chlorite = 2×). Several previous workers used those factors to characterize clays from Cascadia Basin and vicinity (Duncan et al., 1970; Knebel et al., 1968; Karlin, 1980). Errors in such
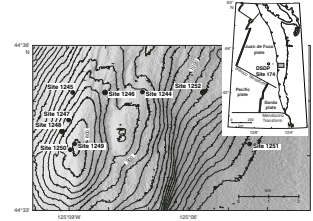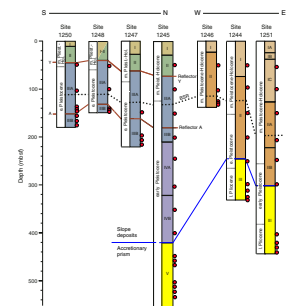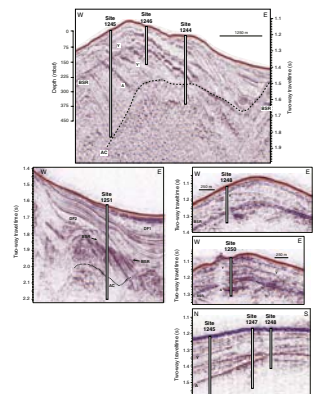
data can be substantial, however, and they change significantly with the absolute abundance by weight of each mineral (Underwood et al., 2003). Results are also affected by differences in sample disaggregation technique, chemical treatments, particle size separation, and the degree of preferred orientation of clay mounts (Moore and Reynolds, 1989; McManus, 1991). Even though data reproducibility might be very good, accuracy is usually no better than ±10% unless the analytical methods include calibration with internal standards. Errors are also smaller if, by good fortune, the absolute proportions of minerals within clay mixtures are close to equal.

Sample Preparation

Isolation of clay-sized fractions started with drying and gentle crushing of the mud/mudstone, after which specimens were immersed in 3% H_2O_2 for at least 24 hr to digest organic matter. We then added ~250 mL of Na-hexametaphosphate solution (concentration of 4 g/1000 mL) and inserted beakers into an ultrasonic bath for several minutes to promote disaggregation and deflocculation. This step (and additional soaking) was repeated until visual inspection indicated complete disaggregation. Washing consisted of two passes through a centrifuge (8200 revolutions per minute [rpm] for 25 min; ~6000g) with resuspension in distilled water after each pass. After transferring the suspended sediment to a 60-mL plastic bottle, each sample was resuspended by vigorous shaking and a 2-min application of a sonic cell probe. The clay-sized splits (<2 μm equivalent settling diameter) were then separated by centrifugation (1000 rpm for 2.4 min; ~320g). Oriented clay aggregates were prepared using the filter-peel method and 0.45-μm membranes (Moore and Reynolds, 1989). The clay aggregates were saturated with ethylene glycol vapor for at least 24 hr prior to XRD analysis, using a closed vapor chamber heated to 60°C in an oven.

X-Ray Diffraction Parameters

The XRD laboratory at the University of Missouri utilizes a Scintag Pad V X-ray diffractometer with CuK_{α} radiation (1.54 Å) and Ni filter. Scans of oriented clay aggregates were run at 40 kV and 30 mA over a scanning range of 2° to 23°2θ, a rate of 1°2θ/min, and a step size of 0.01°2θ. Slits were 0.5 mm (divergence) and 0.2 mm (receiving). We processed the digital data using MacDiff software (version 4.2.5) to establish a baseline of intensity, smooth counts, correct peak positions caused by misalignment of the detector (using the quartz [100] peak at 20.95°2θ; d-value = 4.24 Å), and calculate integrated peak areas (total counts).

Figure F4 shows a representative diffractogram for a clay-sized aggregate. The weighting factors of Biscaye (1965) apply to the integrated areas of a broad smectite (001) peak centered at ~5.3°2θ (d-value = 16.5 Å), the illite (001) peak at ~8.9°2θ (d-value = 9.9 Å), and the chlorite (002) peak at 12.5°2θ (d-value = 7.06 Å). Because of interference between small amounts of kaolinite (001 reflection) and chlorite (002 reflection), we report that relative abundance as chlorite (+ kaolinite). As an indicator of clay diagenesis, the saddle/peak method (Rettke, 1981) was used to calculate the percent expandability of smectite within illite/smectite (I/S) mixed-layer clay.

F4. Representative X-ray diffractogram, p. 11.
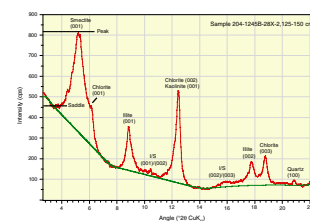
RESULTS

A total of 56 samples of mud and mudstone were analyzed during this investigation. Figures F5, F6, and F7 illustrate how relative abundances of smectite, illite, and chlorite (+ kaolinite) change as a function of depth and stratigraphic unit in the vicinity of Hydrate Ridge. All of the X-ray diffraction data are tabulated in Table T1. For the most part, the results are unremarkable. At Sites 1244, 1245, and 1251, we note a modest increase in the abundance of smectite within deeper stratigraphic intervals that have been interpreted to be part of the Cascadia accretionary complex. On average, the early Pleistocene to Holocene trench slope and slope basin deposits contain 29% smectite (standard deviation = 5.3%), 31% illite (standard deviation = 3.7%), and 40% chlorite (+ kaolinite) (standard deviation = 3.6%). These percentages are entirely consistent with the results of Karlin (1980), who mapped clay mineral abundances using surface sediments from across the continental margin of Oregon and southern Washington.

Late Pliocene to early Pleistocene strata from the underlying accretionary prism show moderate enrichments of smectite with average values of 38% smectite (standard deviation = 3.9%), 27% illite (standard deviation = 2.9%), and 35% chlorite (+ kaolinite) (standard deviation = 2.6%). We attribute this enrichment of expandable clay minerals to detrital point sources associated with the ancestral Columbia River, combined with south-directed transport of hemipelagic suspensions on the floor of Cascadia Basin. As supporting evidence for this interpretation, Karlin (1980) and Knebel et al. (1968) showed that Holocene clays emanating from the mouth of the Columbia River contain more than 50% smectite. Oceanographic currents generally push the Columbia River mud plume toward the north over the continental shelf and slope, but turbidity currents on the floor of Cascadia Basin move sand and smectite-rich suspended sediment toward the south with local funneling through channel-levee complexes (Duncan et al., 1970). DSDP Site 174 is located on the distal edge of Astoria Fan, west of Hydrate Ridge (Fig. F1). The range and average of the relative clay mineral proportions in mud and mudstone samples from that site (Underwood, 2002, in press) are similar to the values reported here for the inferred accretionary complex beneath Hydrate Ridge. Smectite values for older (Pliocene) and finer-grained abyssal plain deposits beneath Astoria Fan are slightly higher with an average abundance of 42% and a maximum of 64% (Underwood, in press). Thus, there seems to have been a temporal change in clay discharge onto the floor of Cascadia Basin in addition to the spatial distribution of point sources.

Among the significant results of shipboard pore water analyses during Leg 204 are the chloride concentration profiles along an east-to-west transect from Site 1252 to Site 1245, which show progressive depletions at depth relative to ocean bottom water (Shipboard Scientific Party, 2003; Torres et al., 2004). This geochemical pattern is consistent with diffusion from a fluid source within deeper-seated sediments of the accretionary complex. In this postulated source area of fluid, a progressive increase in smectite dehydration is driven by an increase in temperature and reaction time with distance from and depth beneath the prism toe. Any effect of changing clay composition seems to be minimal.

In further support of the geochemical interpretations cited above, the XRD data show no evidence of in situ smectite-to-illite diagenesis at Hydrate Ridge. The expandability of the expandable clay ranges from

F5. Percent clay minerals, Sites 1244 and 1245, p. 12.
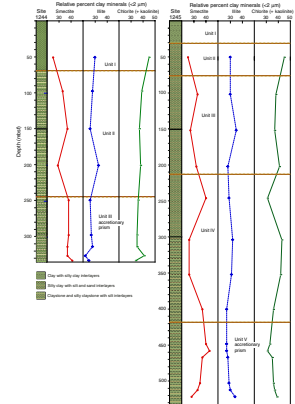
F6. Percent clay minerals, Sites 1246 and 1247, p. 13.
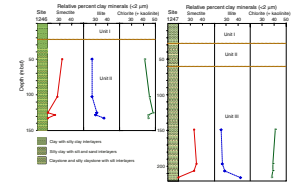
F7. Percent clay minerals, Sites 1248, 1250, and 1251, p. 14.
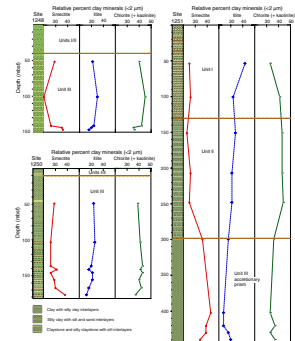
T1. Results of X-ray diffraction analyses, p. 15.

70% to 52% with a mean value of 64% and a standard deviation of 4% (Table T1). There are no trends in the expandability values as a function of depth or depositional age in the sampled lithologies (Table T1). Thus, the smectite appears to be mostly detrital in origin with no diagenetic overprint. This result is not unexpected given the shallow burial depths of most samples. Linear geothermal gradients range from a maximum of 0.061°C/m at Sites 1244 and 1246 to a minimum of 0.052°C/m at Site 1247 (Shipboard Scientific Party, 2003). If one assumes that the gradients remain linear to total depth at each site, this means that the maximum burial temperatures are approximately 24°C at Site 1244, 33°C at Site 1245, and 27°C at Site 1251. To initiate smectite-to-illite diagenesis, burial temperatures need to be within the range of 58°C to 92°C (Freed and Peacor, 1989). Thus, the likelihood of in situ smectite dehydration is remote.

On the other hand, the data presented here document the presence of enough smectite in the accreted sediments beneath Hydrate Ridge to support significant interlayer water release at depths >1000 to 1150 meters below seafloor (mbsf). Bulk-powder XRD data from DSDP Site 174 indicate that the average content of total clay minerals is ~42% by weight (relative to quartz + feldspar + calcite), so the amount of smectite in bulk mudstone averages ~16% with a maximum of ~26%. Given the regional geothermal gradient, the freshened fluids must be migrating from deeper than 1 km. A source at that depth is also consistent with data from analyses of hydrocarbons (Claypool et al., this volume) and strontium isotopes (Teichert et al., 2005).

CONCLUSIONS

The results of X-ray diffraction analysis of clay minerals from the Hydrate Ridge portion of the Cascadia subduction zone are consistent with previous studies of near-surface sediments from the continental margin of Oregon and southern Washington. On average, early Pleistocene to Holocene trench slope and slope basin deposits contain 29% smectite, 31% illite, and 40% chlorite (+ kaolinite). Late Pliocene to early Pleistocene strata from the underlying accretionary prism contain moderately greater amounts of smectite with average values of 38% smectite, 27% illite, and 35% chlorite (+ kaolinite). There is no evidence for in situ diagenetic alteration of the clay minerals, but reaction of smectite at greater depths probably contributes to the documented freshening of pore waters.

ACKNOWLEDGMENTS

REFERENCES

Barnard, W.D., 1978. The Washington continental slope: Quaternary tectonics and sedimentation. *Mar. Geol.,* 27:79–114. doi:10.1016/0025-3227(78)90075-0

Biscaye, P.E., 1965. Mineralogy and sedimentation of recent deep-sea clays in the Atlantic Ocean and adjacent seas and oceans. *Geol. Soc. Am. Bull.,* 76:803–831.

Cook, H.E., Johnson, P.D., Matti, J.C., and Zemmels, I., 1975. Methods of sample preparation and X-ray diffraction data analysis, X-ray Mineralogy Laboratory, Deep Sea Drilling Project, University of California, Riverside. *In* Hayes, D.E., Frakes, L.A., et al., *Init. Repts. DSDP,* 28: Washington (U.S. Govt. Printing Office), 999–1007.

Duncan, J.R., Kulm, L.D., and Griggs, G.B., 1970. Clay mineral composition of late Pleistocene and Holocene sediments of Cascadia Basin, northeastern Pacific Ocean. *J. Geol.,* 78:213–221.

Fisher, A.T., and Underwood, M.B., 1995. Calibration of an X-ray diffraction method to determine relative mineral abundances in bulk powders using matrix singular value decomposition: a test from the Barbados accretionary complex. *In* Shipley, T.H., Ogawa, Y., Blum, P., et al., *Proc. ODP, Init. Repts.,* 156: College Station, TX (Ocean Drilling Program), 29–37.

Freed, R.L., and Peacor, D.R., 1989. Variability in temperature of the smectite/illite reaction in Gulf Coast sediments. *Clays Clay Miner.,* 24:171–180.

Heath, G.R., and Pisias, N.G., 1979. A method for the quantitative estimation of clay minerals in North Pacific deep-sea sediments. *Clays Clay Miner.,* 27:175–184.

Johnson, L.J., Chu, C.H., and Hussey, G.A., 1985. Quantitative clay mineral analysis using simultaneous linear equations. *Clays Clay Miner.,* 33:107–117.

Karlin, R., 1980. Sediment sources and clay mineral distributions off the Oregon coast. *J. Sediment. Petrol.,* 50:543–560.

Knebel, H.J., Kelly, J.C., and Whetten, J.T., 1968. Clay minerals of the Columbia River: a qualitative, quantitative and statistical evaluation. *J. Sediment. Petrol.,* 38:600–611.

Kulm, L.D., and Fowler, G.A., 1974. Oregon continental margin structure and stratigraphy: a test of the imbricate thrust model. *In* Burke, C.A., and Drake, C.L. (Eds.), *The Geology of Continental Margins:* New York (Springer), 261–284.

Kulm, L.D., and Scheidegger, K.F., 1979. Quaternary sedimentation on the tectonically active Oregon continental slope. *In* Doyle, L.J., and Pilkey, O.H. (Eds.), *Geology of Continental Slopes.* Spec. Publ.—Soc. Econ. Paleontol. Mineral., 27:247–263.

MacKay, M.E., Moore, G.F., Cochrane, G.R., Moore, J.C., and Kulm, L.D., 1992. Landward vergence and oblique structural trends in the Oregon margin accretionary prism: implications and effect on fluid flow. *Earth Planet. Sci. Lett.,* 109:477–491. doi:10.1016/0012-821X(92)90108-8

McManus, D.A., 1991. Suggestions for authors whose manuscripts include quantitative clay mineral analysis by X-ray diffraction. *Mar. Geol.,* 98:1–5. doi:10.1016/0025-3227(91)90030-8

Moore, C.A., 1968. Quantitative analysis of naturally occurring multicomponent mineral systems by X-ray diffraction. *Clays Clay Miner.,* 16:325–336.

Moore, D.M., and Reynolds, R.C., Jr., 1989. *X-Ray Diffraction and the Identification and Analysis of Clay Minerals:* Oxford (Oxford Univ. Press).

Rettke, R.C., 1981. Probable burial diagenetic and provenance effects on Dakota Group clay mineralogy, Denver Basin. *J. Sediment. Petrol.,* 51:541–551.

Shipboard Scientific Party, 1994a. Site 891. *In* Westbrook, G.K., Carson, B., Musgrave, R.J., et al., *Proc. ODP, Init. Repts.,* 146 (Pt. 1): College Station, TX (Ocean Drilling Program), 241–300.

Shipboard Scientific Party, 1994b. Site 892. *In* Westbrook, G.K., Carson, B., Musgrave, R.J., et al., *Proc. ODP, Init. Repts.,* 146 (Pt. 1): College Station, TX (Ocean Drilling Program), 301–378.

Shipboard Scientific Party, 2003. Leg 204 summary. *In* Tréhu, A.M, Bohrmann, G., Rack, F.R., Torres, M.E., et al., *Proc. ODP, Init. Repts.,* 204 [Online]. Available from World Wide Web: <**http://www-odp.tamu.edu/publications/204_IR/chap_01/chap_01.htm**>. [Cited 2005-09-13]

Teichert, B.M.A., Torres, M.E., Bohrmann, G., and Eisenhauer, A., 2005. Fluid sources, fluid pathways and diagenetic reactions across an accretionary prism revealed by Sr and B geochemistry. *Earth Planet. Sci. Lett.,* 239:106–121. **doi:10.1016/j.epsl.2005.08.002**

Torres, M.E., Teichert, B.M.A., Tréhu, A.M., Borowski, W., and Tomaru, H., 2004. Relationship of pore water freshening to accretionary processes in the Cascadia margin: fluid sources and gas hydrate abundance. *Geophys. Res. Lett.,* 31:L22305. **doi:10.1029/2004GL021219**

Underwood, M.B., Basu, N., Steurer, J., and Udas, S., 2003. Data report: Normalization factors for semiquantitative X-ray diffraction analysis, with application to DSDP Site 297, Shikoku Basin. *In* Mikada, H., Moore, G.F., Taira, A., Becker, K., Moore, J.C., and Klaus, A. (Eds.), *Proc. ODP, Sci. Results,* 190/196, 1–28 [Online]. Available from World Wide Web: <**http://www-odp.tamu.edu/publications/190196SR/VOLUME/CHAPTERS/203.PDF**>. [Cited 2005-09-13]

Underwood, M.B., 2002. Strike-parallel variations in clay minerals and fault vergence in the Cascadia subduction zone. *Geology,* 30:155–158. **doi:10.1130/0091-7613(2002)030<0155:SPVICM>2.0.CO;2**

Underwood, M.B., in press. Sediment inputs to subduction zones: why lithostratigraphy and clay mineralogy matter. *In* Dixon, T., and Moore, J.C. (Eds.), *The Seismogenic Zone of Subduction Thrust Faults:* New York (Columbia Univ. Press).

Underwood, M.B., Hoke, K.D., Fisher, A.T., Davis, E.E., Giambalvo, E., Zühlsdorff, L., and Spinelli, G.A., 2005. Provenance, stratigraphic architecture, and hydrogeologic influence of turbidites on the mid-ocean ridge flank of northwestern Cascadia Basin, Pacific Ocean. *J. Sediment. Res.,* 75(1):149-164. **doi:10.2110/jsr.2005.012**

Figure F1. Index map with location of Hydrate Ridge study area and drill sites occupied during ODP Leg 204. Note the location of Deep Sea Drilling Project (DSDP) Site 174. Modified from Shipboard Scientific Party (2003).
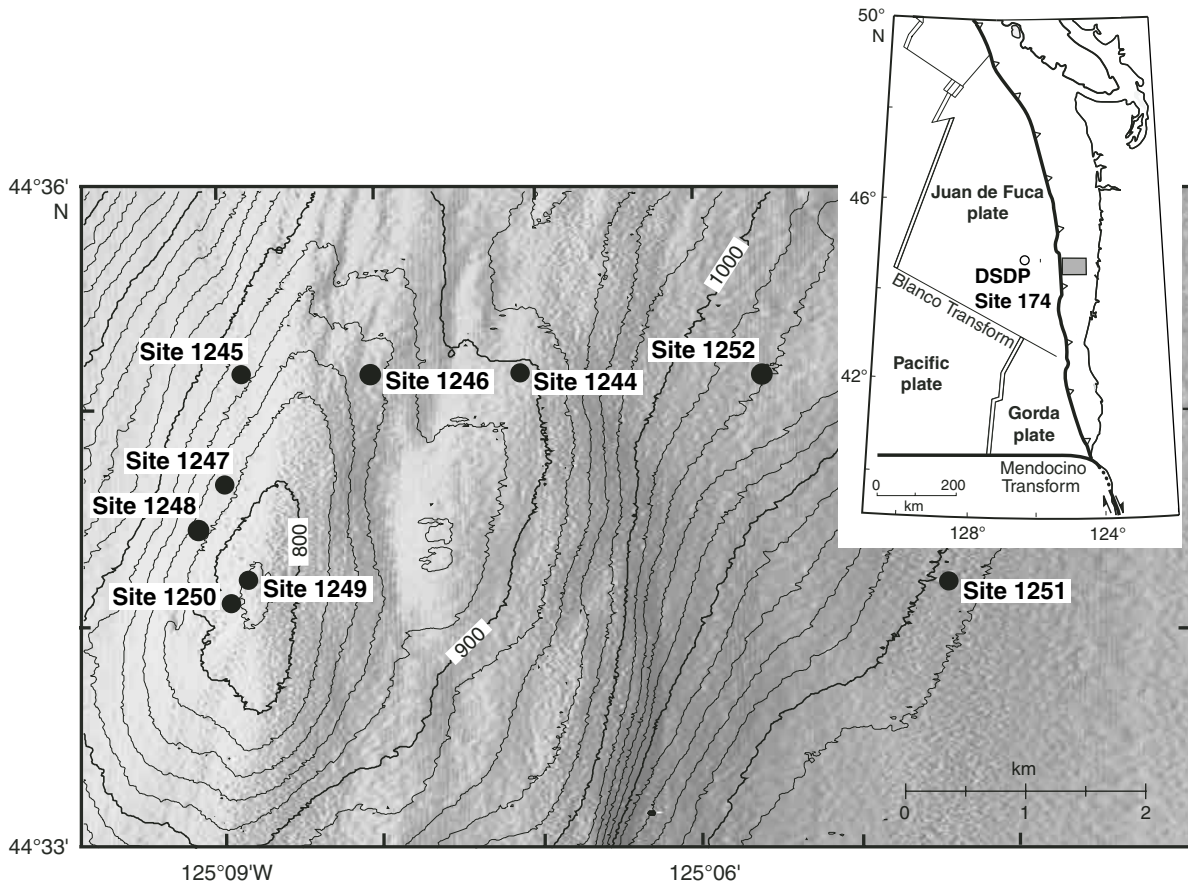
Figure F2. Correlation of lithostratigraphic units recovered by drilling at Hydrate Ridge. See Figure F1, p. 8, for locations of sites. Red dots show positions of samples analyzed by X-ray diffraction. Reflectors Y and A have been correlated on seismic-reflection profiles (see Fig. F3, p. 10). BSR = bottom-simulating reflector. Modified from Shipboard Scientific Party (2003).
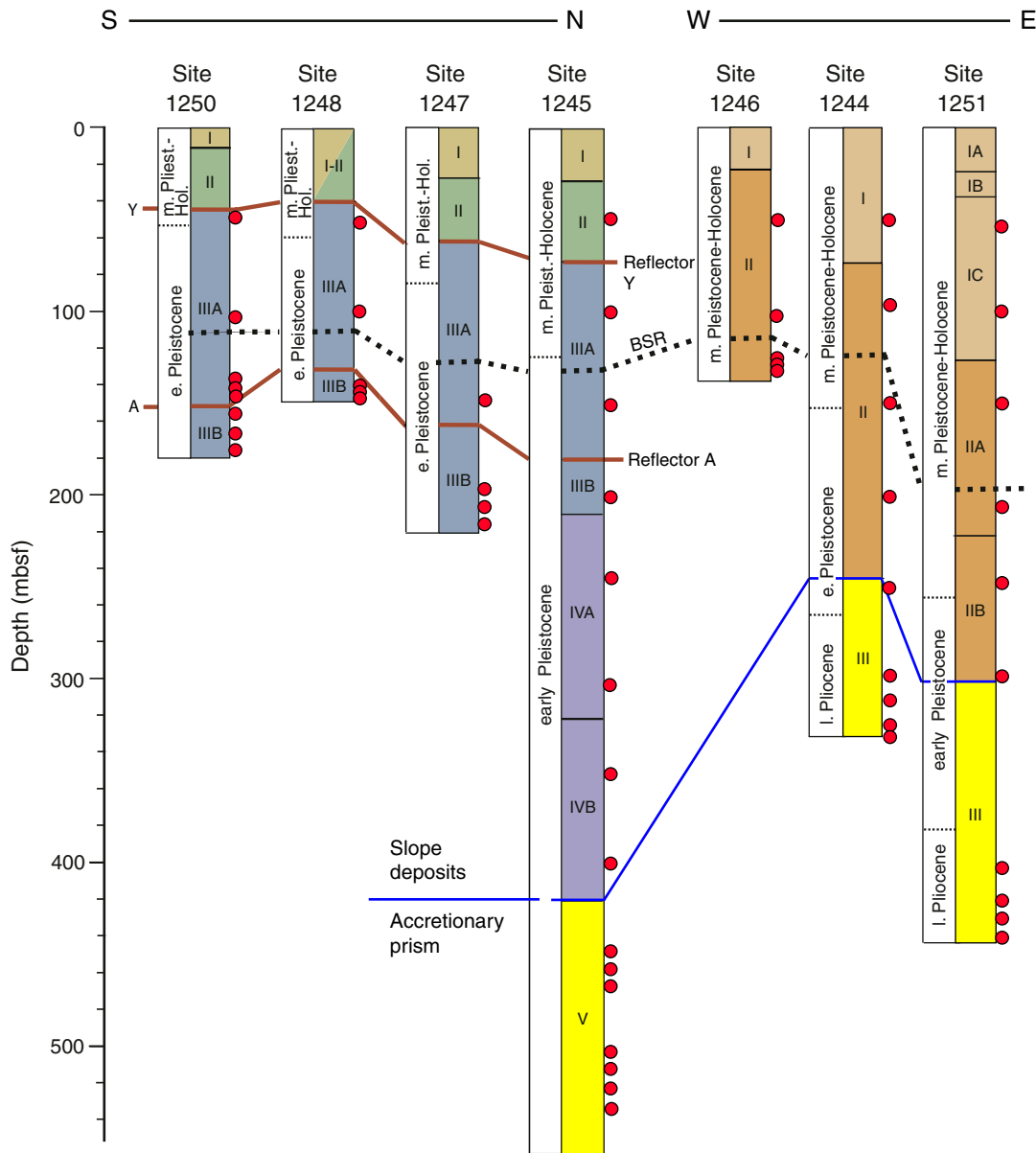
Figure F3. Seismic reflection profiles showing site locations and depths of penetration for cores analyzed as part of this X-ray diffraction study. See Figure F2, p. 9, for depth distribution of samples. BSR = bottom-simulating reflector. DF1 and DF2 are debris-flow units. AC = accretionary complex. Modified from Shipboard Scientific Party (2003).
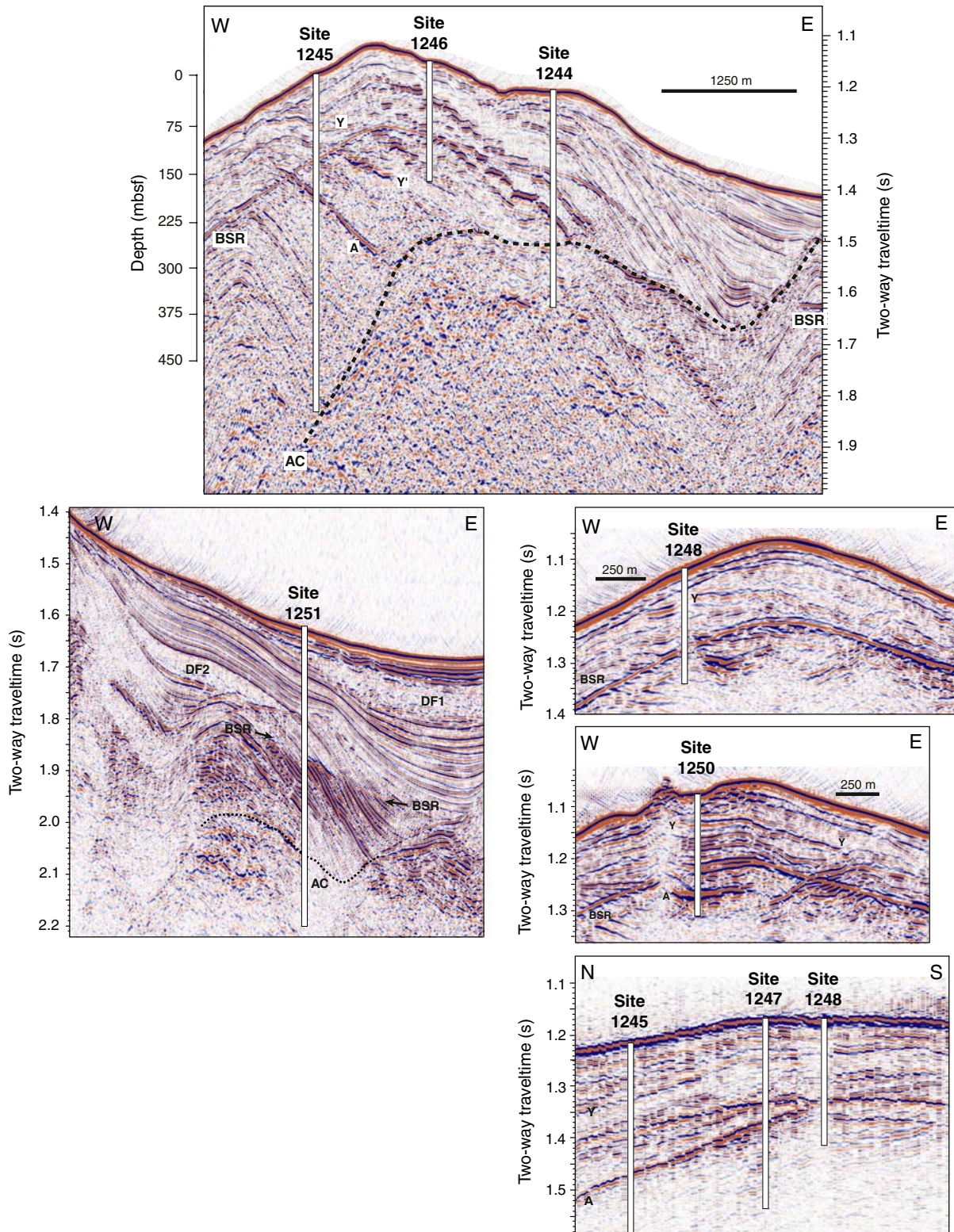
Figure F4. Representative X-ray diffractogram showing the peaks used for calculations of relative mineral abundance: smectite (001), illite (001), and chlorite (002). Calculations employed the weighting factors of Biscaye (1965). Intensities (counts per second [cps]) of the saddle and peak of the smectite (001) reflection were used to calculate percent expandability, following the method of Rettke (1981). I/S = illite/smectite.
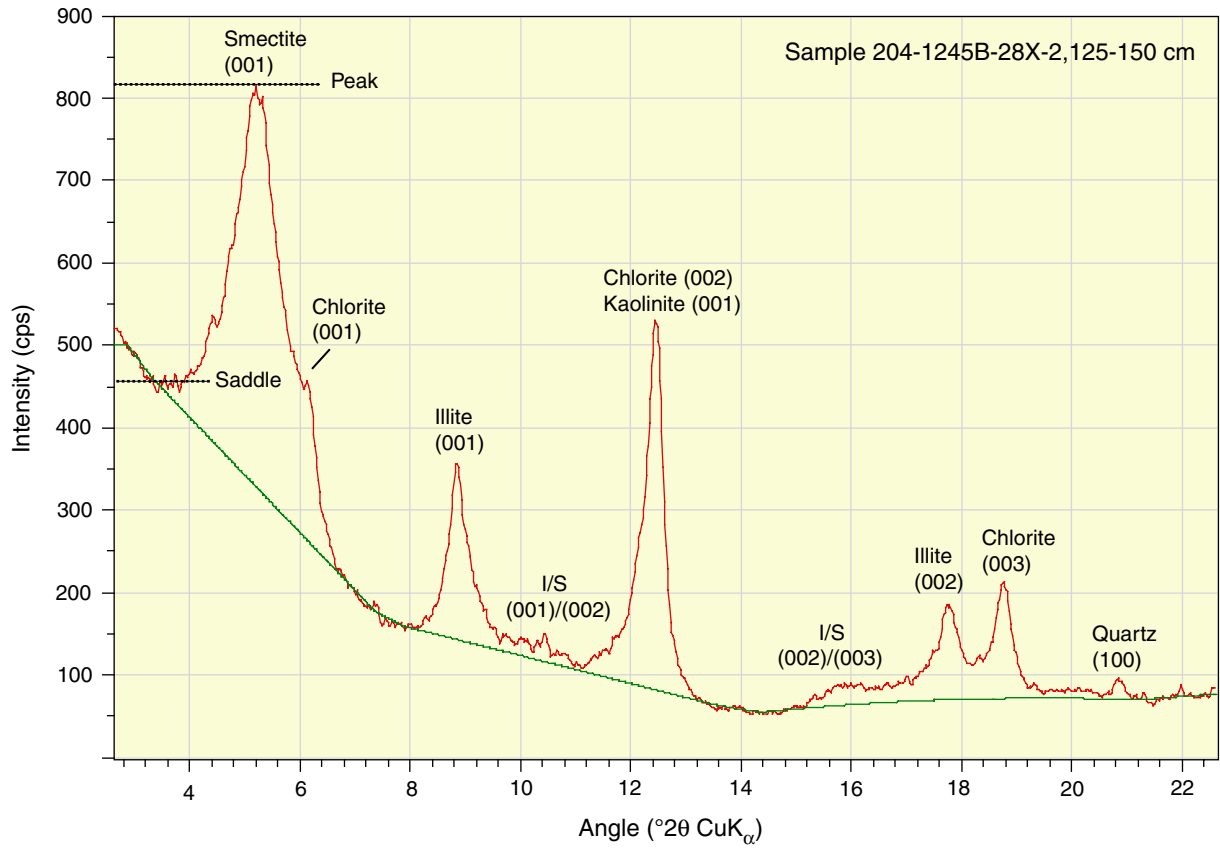
Figure F5. Relative abundances of smectite, illite, and chlorite (+ kaolinite) plotted as a function of depth at ODP Sites 1244 and 1245. See Figure F1, p. 8, for locations and Table T1, p. 15, for X-ray diffraction peak area values.
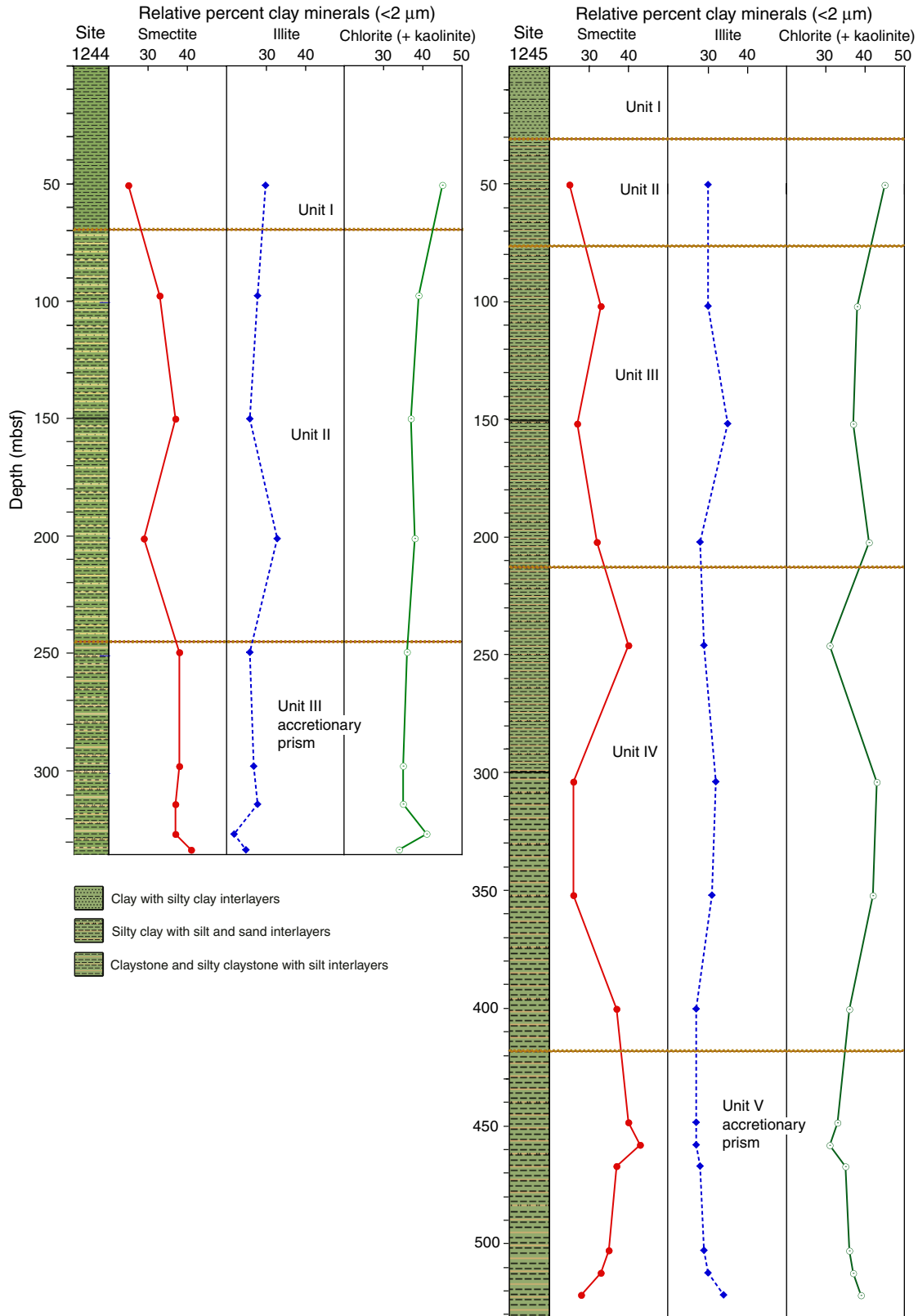
Figure F6. Relative abundances of smectite, illite, and chlorite (+ kaolinite) plotted as a function of depth at ODP Sites 1246 and 1247. See Figure F1, p. 8, for locations and Table T1, p. 15, for X-ray diffraction peak area values.
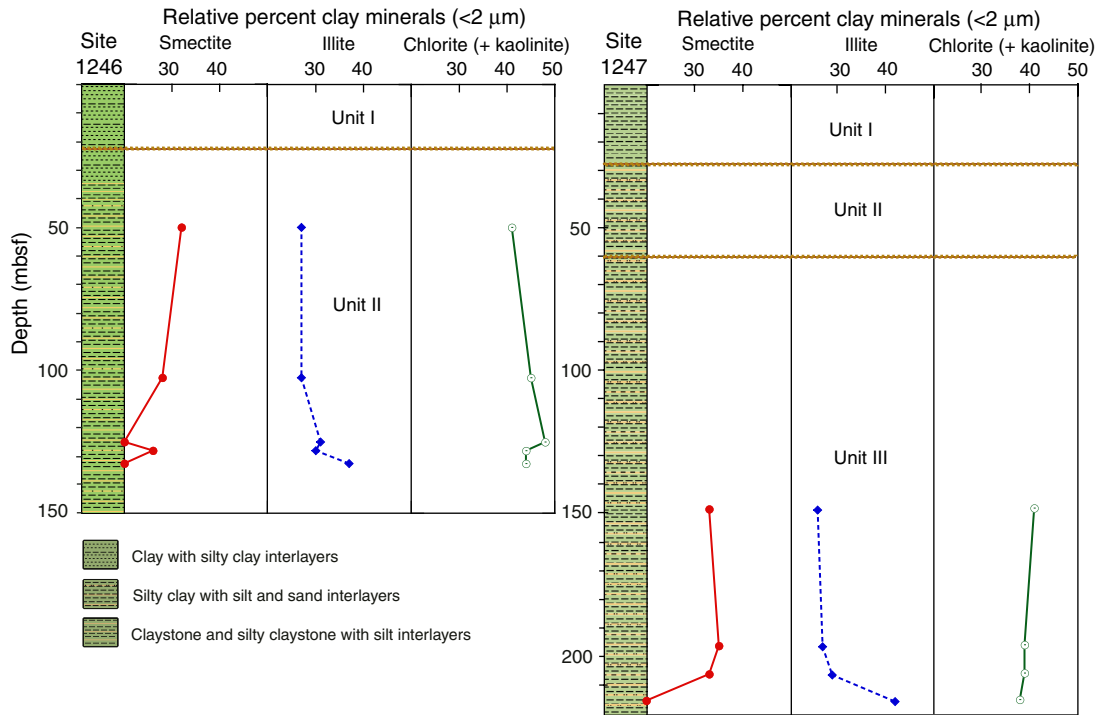
Figure F7. Relative abundances of smectite, illite, and chlorite (+ kaolinite) plotted as a function of depth at ODP Sites 1248, 1250, and 1251. See Figure F1, p. 8, for locations and Table T1, p. 15, for X-ray diffraction peak area values.
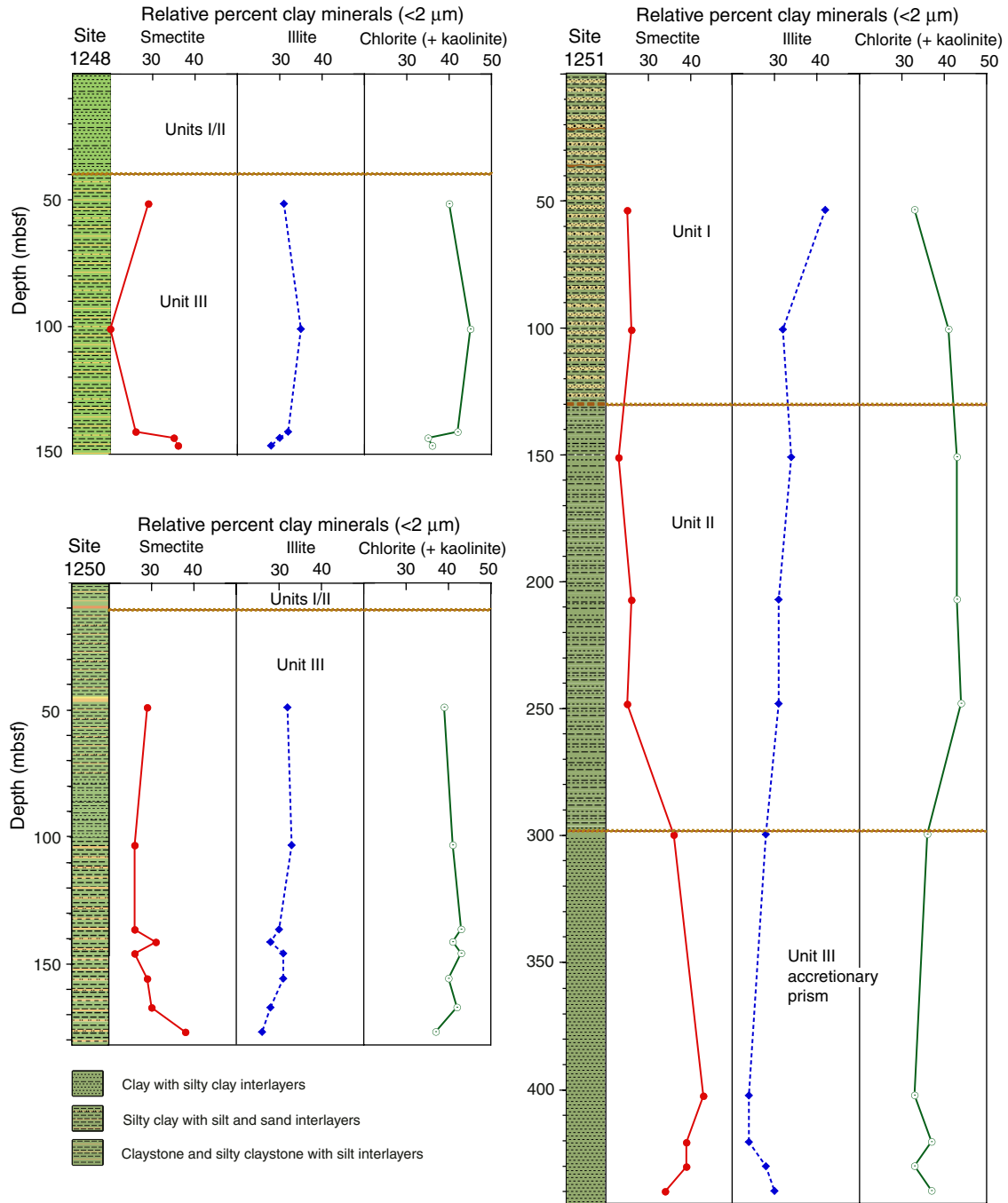
Table T1. Results of X-ray diffraction analyses, <2-µm size fraction, Hydrate Ridge, Cascadia margin.

Core, section, interval top (cm)	Depth (mbsf)	Unit	Age (Ma)	X-ray diffraction peak area (total counts)			Relative % (Biscaye factors)			Illite/smectite mixed-layer clay			
				Smectite (001)	Illite (001)	Chlorite (002)	Smectite	Illite	Chlorite + kaolinite	S(001) saddle	S(001) peak	Saddle/ peak	% Expand
204-1244C-													
6H-5, 135	50.71	I	<0.27	21,044	6,283	18,690	25	30	45	347	488	0.71	63
11H-5, 135	97.58	II	0.46–1.00	42,460	9,089	25,030	33	28	39	372	637	0.58	68
19X-5, 85	149.85	II	0.46–1.00	49,875	8,805	24,592	37	26	37	456	791	0.58	69
25X-3, 135	200.75	II	0.46–1.00	40,320	11,469	26,427	29	33	38	386	594	0.65	66
30X-3, 130	249.00	III	1.59–1.67	32,274	5,450	15,047	38	26	36	375	567	0.66	65
35X-3, 130	297.33	III	1.70–2.78	41,484	7,304	19,166	38	27	35	432	667	0.65	66
37X-1, 130	313.50	III	1.70–2.78	34,141	6,442	16,352	37	28	35	320	533	0.60	68
38X-3, 130	326.20	III	>2.78	30,781	4,537	17,166	37	22	41	335	534	0.63	67
39X-1, 130	332.80	III	>2.78	21,260	3,222	8,617	41	25	34	300	413	0.73	62
204-1245B-													
6H-2, 140	50.40	II	<0.27	29,597	9,029	27,403	25	30	45	392	571	0.69	64
11H-5, 140	101.87	III	0.46–1.00	36,155	8,186	20,842	33	30	38	406	633	0.64	66
18X-2, 113	151.73	III	1.00–1.20	36,226	11,712	24,471	27	35	37	460	647	0.71	63
23X-5, 125	201.95	III	1.00–1.20	29,563	6,448	19,042	32	28	41	310	500	0.62	67
28X-2, 125	245.68	IV	1.00–1.20	59,522	11,029	23,056	40	29	31	451	817	0.55	70
35X-2, 125	303.55	IV	1.20–1.59	28,799	8,833	23,892	26	32	43	355	515	0.69	64
40X-2, 125	351.65	IV	1.20–1.59	19,369	5,846	15,793	26	31	42	335	441	0.76	60
45X-2, 125	399.85	IV	1.20–1.59	29,402	5,431	14,572	37	27	36	356	508	0.70	63
51X-2, 125	447.95	V	1.20–1.59	39,408	6,561	15,892	40	27	33	383	599	0.64	66
52X-2, 125	457.45	V	1.20–1.59	53,495	8,341	19,270	43	27	31	469	760	0.62	67
53X-2, 125	466.51	V	1.20–1.59	42,499	8,080	20,540	37	28	35	344	583	0.59	68
204-1245E-													
4R-1, 130	502.20	V	1.20–1.59	20,093	4,133	10,295	35	29	36	289	395	0.73	62
5R-1, 122	511.72	V	1.20–1.59	19,585	4,458	11,149	33	30	37	312	413	0.76	60
6R-1, 85	521.05	V	>1.59	19,006	5,760	13,175	28	34	39	307	401	0.77	60
7R-1, 132	531.12	V	>1.59										
204-1246B-													
6H-5, 140	50.00	II	<0.27	26,559	5,733	16,973	32	27	41	312	493	0.63	66
12H-2, 140	102.60	II	0.27–0.46	18,820	4,622	15,481	28	27	45	312	426	0.73	62
15H-2, 140	125.15	II	>0.46	14,032	5,456	16,848	20	31	48	298	365	0.82	57
15H-4, 140	128.15	II	>0.46	18,926	5,323	15,908	26	30	44	297	400	0.74	61
16H-2, 140	132.70	II	>0.46	19,886	9,136	21,797	20	37	44	349	454	0.77	60
204-1247B-													
20X-3, 130	148.50	III	1.00–1.20	32,407	6,423	20,304	33	26	41	398	606	0.66	65
25X-3, 130	196.33	III	>1.59	37,749	7,314	21,082	35	27	39	421	657	0.64	66
26X-3, 130	206.20	III	>1.59	31,746	7,017	18,840	33	29	39	388	582	0.67	65
27X-3, 130	215.50	III	>1.59	12,636	6,719	12,304	20	42	38	289	343	0.84	55
204-1248C-													
6H-3, 129	51.05	III	0.46–1.59	30,280	7,918	20,392	29	31	40	386	571	0.68	64
11H-4, 122	100.36	III	0.46–1.59	9,975	4,386	11,475	20	35	45	242	288	0.84	55
16H-3, 135	140.85	III	>1.59	24,306	7,360	19,525	26	32	42	339	496	0.68	64
17X-1, 130	143.30	III	>1.59	42,441	8,980	20,923	35	30	35	420	671	0.63	67
17X-3, 135	146.30	III	>1.59	31,389	6,228	16,051	36	28	36	372	571	0.65	66
204-1250C-													
6H-5, 118	48.95	III	<0.27	22,729	6,292	15,617	29	32	39	350	463	0.76	60
13H-2, 130	103.19	III	>1.59	19,172	6,051	15,060	26	33	41	323	438	0.74	61
17H-3, 130	136.30	III	>1.59	22,053	6,295	18,175	26	30	43	276	419	0.66	65
19X-2, 130	141.30	III	>1.59	29,448	6,701	19,881	31	28	41	344	511	0.67	65
19X-5, 130	145.75	III	>1.59	21,762	6,466	18,000	26	31	43	339	448	0.76	60
204-1250F-													
11X-2, 98	155.68	III	>1.59	28,195	7,403	19,054	29	31	40	348	509	0.68	64
12X-3, 125	167.05	III	>1.59	25,108	5,751	17,107	30	28	42	364	504	0.72	62
13X-3, 125	176.65	III	>1.59	31,789	5,466	15,459	38	26	37	380	575	0.66	65
204-1251B-													
6H-5, 131	53.61	I	0.09–0.27	6,488	2,756	4,312	25	42	33	222	254	0.87	52
11H-5, 70	100.61	I	0.09–0.27	27,421	8,463	21,510	26	32	41	290	433	0.67	65
17H-5, 80	150.90	II	0.27–0.46	20,631	7,740	19,104	23	34	43	280	402	0.70	64
26X-2, 130	207.00	II	0.46–1.00	23,355	6,905	19,080	26	31	43	330	452	0.73	62
30X-4, 110	248.00	II	0.46–1.00	18,188	5,614	15,975	25	31	44	317	425	0.75	61
36X-5, 80	299.40	II	1.59–1.67	41,547	8,092	20,836	36	28	36	412	651	0.63	66
49X-3, 130	402.20	III	1.7–2.0	27,024	3,802	10,390	43	24	33	320	471	0.68	64
51X-3, 130	420.50	III	1.7–2.0	39,292	6,029	18,865	39	24	37	401	631	0.64	66
52X-3, 130	430.10	III	1.7–2.0	33,853	5,976	13,990	39	28	33	367	569	0.64	66
53X-3, 130	439.78	III	>2.0	36,342	7,948	19,810	34	30	37	348	570	0.61	67